

Space-based multilateration for a GNSS-independent aircraft localisation[☆]

Mauro Leonardi^{ID*}, Giulio Sidoretti^{ID}, Edoardo Navarra^{ID}, Mahsa Mohebbi^{ID}

University of Rome “Tor Vergata”, Via del Politecnico, 1, Rome, 00133, Italy

ARTICLE INFO

Keywords:

Air traffic control
Multilateration
ADS-B
CRLB
LEO satellite
Independent localisation
LEO constellation

ABSTRACT

Modern Air Traffic Control (ATC) relies on the Automatic Dependent Surveillance–Broadcast (ADS-B) system, which transmits GNSS-based aircraft positions (computed onboard) to the ground. While ADS-B is key to future Air Traffic Management (ATM), its dependence on GNSS makes it vulnerable to failures and cyber-attacks. For this reason, ground-based systems are currently used to validate ADS-B data, but they are unavailable in remote areas, such as the ocean.

This paper proposes a Low Earth Orbit (LEO) satellite constellation performing multilateration (MLAT) on ADS-B signals to provide GNSS-independent position estimates. Unlike classical ground-based multilateration, the space context introduces challenges such as limited visibility, poor geometry, ill-conditioning, and synchronisation issues. To address these limitations, two possible solutions are presented and evaluated: (i) a combination of Time of Arrival (TOA) with additional measurements, such as Frequency of Arrival (FOA) and Angle of Arrival (AOA); (ii) an improved and optimised receiver antenna to obtain larger coverage of the satellites. In both cases, the proposed architecture comprises LEO satellites equipped with ADS-B phased array antennas, useful for obtaining multiple beams with different footprints on the ground.

The system localisation performance is evaluated using the Cramér–Rao Lower Bound (CRLB). Simulations over the Atlantic Ocean assess different measurement combinations and constellation configurations.

The results show that, with the appropriate design, the system achieves a localisation accuracy that completely meets the requirements of air traffic control en-route (i.e., 350 m horizontal RMS error).

1. Introduction

Air Traffic Control (ATC) is a central component of the broader Air Traffic Management (ATM) framework. Its primary objective is to prevent collisions between aircraft while ensuring an orderly and efficient flow of air traffic. ATC relies on a combination of technologies, procedures, and human expertise, and is also essential due to the increasingly congested nature of controlled airspace, particularly in terminal areas and along major international routes. Historical studies have shown that ATC, together with onboard and ground safety-net systems, can reduce the risk of collision by up to three orders of magnitude, making air transport one of the safest modes of travel [1,2].

Traditionally, surveillance within ATC has been provided by Secondary Surveillance Radar (SSR), which uses aircraft transponders to retrieve position and identity information. However, SSR-based systems have inherent limitations in update rate, coverage, and scalability [3]. To overcome these challenges, the aviation industry adopted the Communication, Navigation, Surveillance and Air Traffic Management (CNS/ATM) framework, which supports SSR with new technologies. A key advancement in this modernisation effort is the deployment

of Automatic Dependent Surveillance Broadcast (ADS-B) [3]. In ADS-B, aircraft periodically broadcast their state vector (position, velocity, identification, and other data) over 1090 MHz using the Mode S protocol. This information is primarily derived from onboard Global Navigation Satellite Systems (GNSS) and can be received by ground stations and other aircraft, enabling higher update rates and more accurate tracking than traditional radar. These capabilities allow for reduced separation minima, improved situational awareness, and more efficient and environmentally sustainable flight trajectories [3].

Despite these benefits, conventional ADS-B systems have two major limitations. First, ADS-B is not an independent surveillance system; it relies entirely on GNSS-derived position data, making it vulnerable to jamming, spoofing, or onboard system failures. Second, ground-based ADS-B infrastructure is often unavailable or impractical to deploy in remote and oceanic regions, limiting coverage and requiring large separation minima for aircraft operating in these areas. ADS-C [4,5], Automatic Dependent Surveillance-Contract, is widely used to provide surveillance in remote and oceanic airspace. However, separation minima can be further reduced with space-based ADS-B, which enables

[☆] This article is part of a Special issue entitled: ‘76th IAC invited only’ published in Acta Astronautica.

* Corresponding author.

E-mail address: mauro.leonardi@uniroma2.it (M. Leonardi).

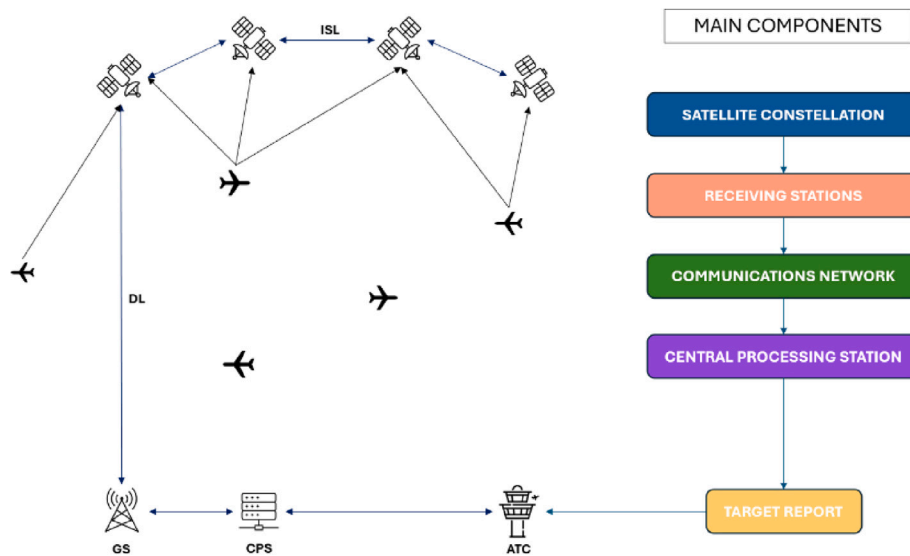


Fig. 1. E-MLAT architecture.

more frequent and near real-time aircraft position updates, especially in high-traffic transoceanic corridors, such as the North Atlantic, connecting North America and Europe. An existing ADS-B via satellite solution is the one offered by Aireon [6], but it is still fully dependent on GNSS.

To address these challenges, the Space-based composite ADS-B and multilateration system validation through scalable simulations (SAT-ERA) project [7] proposes a novel surveillance architecture: a composite space-based ADS-B Enhanced Multilateration (E-MLAT) system using a constellation of Low Earth Orbit (LEO) satellites. The system combines ADS-B reception and multilateration techniques based on Time of Arrival (TOA), Frequency of Arrival (FOA), and Angle of Arrival (AOA) measurements, enabling GNSS-independent aircraft localisation and ADS-B data validation. The SAT-ERA final goal is offering a robust, redundant, and global surveillance capability, supporting optimised, fuel-efficient routing even in remote and oceanic areas, while improving safety, integrity, and resilience in air traffic surveillance.

In this framework, the scope of this work is to evaluate: (i) the performance advantages provided by the addition of new measurements on the satellites (FOA and AOA), and/or (ii) those obtained when using tailored receiving antennas with improved performance that allow the satellites to receive ADS-B messages from farther aircraft, increasing the number of available MLAT measurements for each aircraft.

The rest of the paper is organised as follows: Section 2 introduces the concept of space-based E-MLAT; Section 3 presents the problem formulation; Section 4 contains the Cramér–Rao Lower Bound (CRLB) formulation for E-MLAT; Section 5 shows the simulation and performance evaluation; finally, Section 6 concludes the paper.

2. Space-based E-MLAT main concept

SATERA proposes a constellation of satellites in LEO orbit to receive ADS-B data from aircraft. The ADS-B information broadcasted by the aircraft will be received on-board each satellite of the constellation by specific equipment that measures one or more characteristics of the electromagnetic waves carrying ADS-B messages (e.g., TOA, AOA, and FOA). This information will then be relayed between the different satellites via Inter-Satellite Link (ISL) and sent through a downlink (DL) connection to a Central Processing Station (CPS) on the ground. As the space channel is harsh and quite band-limited, appropriate data encoding (including compression) and routing algorithms will be used to prevent the measured data from being affected by channel noise and network congestion, thus ensuring that the required information reaches the CPS on time to be properly processed. Once the data reach

the CPS, they will be processed using multilateration techniques to estimate the aircraft's position [8–10]. This estimation will be compared with the position reported in the ADS-B messages and an integrity indicator will be added to the ADS-B Target Report.

Finally, both reports (ADS-B and E-MLAT) will be integrated into the ATM surveillance chain for ATC purposes (Fig. 1).

In the development of space-based MLAT systems, several technical challenges arise that differ significantly from those encountered in ground-based implementations. These challenges must be addressed to ensure the accurate determination of aircraft positions, particularly in scenarios where space-based ADS-B data need to be supplemented or verified.

One of the primary issues is related to satellite positioning. While satellites can use onboard GNSS receivers to determine their own position, highly accurate, non-GNSS-based orbit determination techniques are necessary. This is because GNSS-derived satellite positions may contain errors, and these errors could propagate into the multilateration process if not properly checked. For this reason, non-GNSS-based methods are needed to ensure that the MLAT data can effectively validate the integrity of the aircraft position information broadcast through ADS-B signals.

Another crucial factor is synchronisation. In ground-based MLAT systems, synchronisation between receivers is essential to deliver highly accurate position data [11]. However, achieving this synchronisation in space-based systems is far more complex than on ground-based systems. In fact, synchronisation techniques suitable for ground systems cannot be implemented directly in the space environment. As a result, new architectures tailored to space-based operations, potentially incorporating non-GNSS synchronisation mechanisms, must be developed.

The communication subsystem also plays a significant role in space-based MLAT performance. In terrestrial systems, communication latency and network congestion are typically negligible unless centralised synchronisation mechanisms are in use. However, in space-based systems, where communication relies on ISLs, latency and congestion could significantly degrade system performance. These challenges are compounded by the fact that the same communication infrastructure may be used for multiple purposes, such as supporting both the ADS-B system and pilot-to-controller communications. Therefore, carefully designed network architectures and protocols must be selected to mitigate these issues and ensure that communication delays do not adversely affect MLAT accuracy.

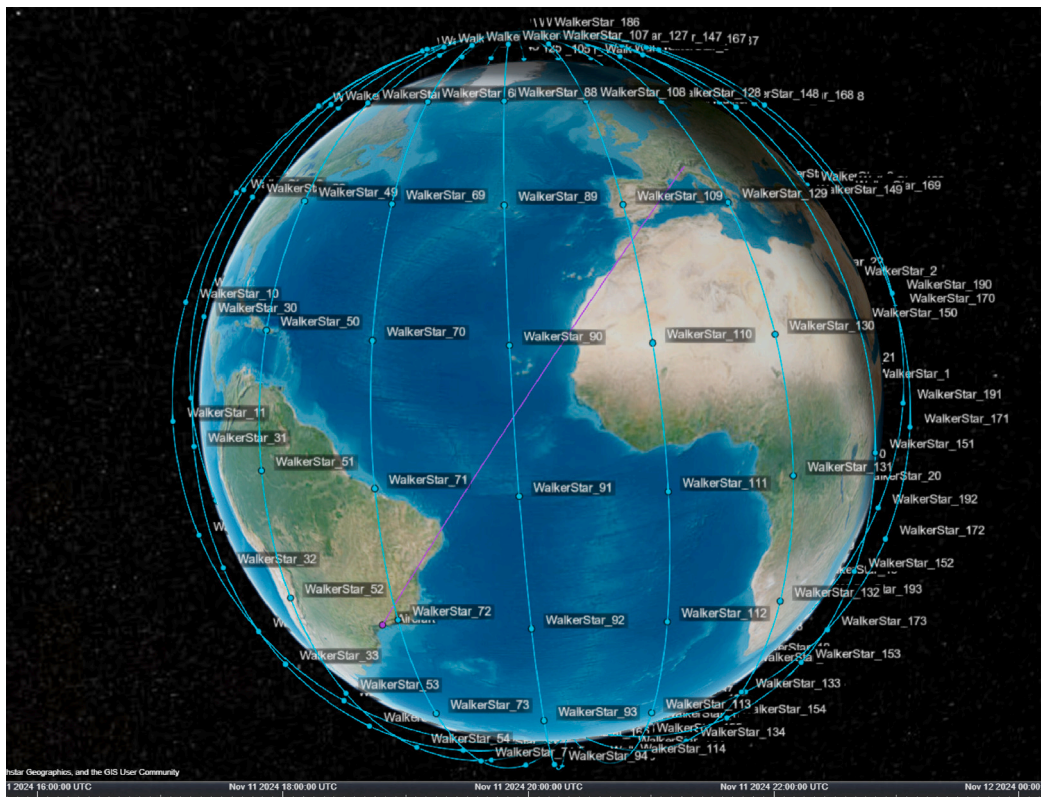


Fig. 2. SATERA constellation.

Table 1
Constellation parameters.

Constellation parameter	Value
Inclination	86°
Orbital altitude	500 km
Total number of satellites	200
Number of orbital planes	10
Number of satellites per orbital plane	20
Orbital phasing	0°

Additionally (and more important for this work), the inverse MLAT problem in space is often ill-conditioned and can suffer from numerical instability due to factors such as poor Dilution of Precision (DOP), low Signal to Noise Ratio (SNR), and uncertainty in receiver positions. To overcome these issues, the space-based MLAT system must deploy satellite constellations with sufficient coverage overlap and/or exploit enhanced position determination algorithms through additional measurements beyond conventional TOA, such as AOA and FOA of the ADS-B message.

Considering these differences, E-MLAT systems have been proposed as a solution. E-MLAT represents an advanced form of MLAT that integrates additional measurements and optimised algorithms to address the limitations imposed by the space environment. By leveraging these enhanced techniques, E-MLAT systems aim to provide more reliable aircraft position data, even under the demanding conditions of space-based surveillance.

2.1. Constellation

In a space-based MLAT system, the receiving stations are integrated into the constellation satellites. As a result, the accuracy of the computed aircraft position depends on the relative geometry and motion of the satellites and the aircraft—as well as the number of satellites within reception range of the aircraft’s ADS-B transmitter.

To meet required performance levels, the constellation must be designed with orbits and revisit times that guarantee sufficient coverage over the area of interest for SATERA, which is between the latitudes 70°N and 70°S. This design must strike a balance between positioning accuracy, resource efficiency (minimising satellite number), and network connectivity.

The proposed LEO satellite constellation (Fig. 2) follows a Walker Star pattern with an inclination of 86° and an orbital altitude of 500 km. The constellation consists of 200 satellites distributed across 10 orbital planes, resulting in 20 satellites per plane. The orbit phase has been set to 0°. This configuration was chosen to facilitate the routing of data across the ISL-based network: a phasing equal to 0° means that a satellite on an orbital plane will see the satellite from the next orbital plane always at the same angle. Moreover, this constellation has been chosen to ensure that at least four satellites are in view in the coverage area of the SATERA system. The constellation parameters are summarised in Table 1.

2.2. Satellite ADS-B sensor

Each receiving station onboard the satellites is responsible for intercepting ADS-B signals transmitted by the aircraft and measuring their physical characteristics. The stations will include a radio front-end to capture 1090 MHz ADS-B messages, down-convert them for digitisation, and extract parameters such as TOA, Doppler shift, and AOA. A core element of this architecture is the use of a phased array antenna for the implementation of Digital Beamforming (DBF), which allows the receiver to combine signals from multiple antenna elements in a coherent and adaptive manner. The implementation of DBF for a satellite-based ADS-B receiver is illustrated in Fig. 3. This payload consists of an array antenna with multiple elements feeding a coherent multi-channel receiver, along with the necessary Radio Frequency (RF) front-end and digital processing stages. The design enables precise extraction of signal time, frequency and angle (TOA, FOA, AOA). In the DBF configuration,

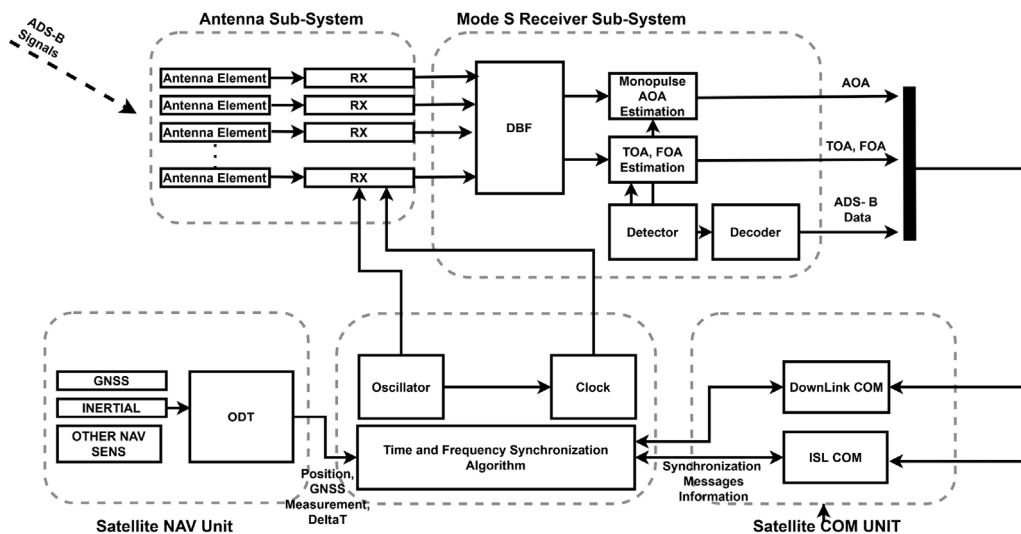


Fig. 3. ADS-B sensor architecture.

Table 2
SATERA Satellite main parameters.

SATERA Satellite parameter	Value
ADS-B Receiver instantaneous band	8 MHz
ADS-B Receiver sensitivity (accounting for receiver noise, internal losses and $SNR_{min} = 10$ dB)	-97 dBm
TOA rx error (std) (SNR between 10–30 dB)	15 ns
FOA rx error (std) (NR between 10–30 dB)	500 Hz
AOA rx error (std) (Considering the antenna dimension and typical 10 dB SNR)	0.01745 rad
Antenna Gain (depending on the selected antenna)	12–17 dBi
Satellite position error	≈ 0.99 m
Satellite velocity error	≈ 0.11 m/s
Satellite attitude error	≈ 40 μ rad
Satellite clock time bias error	<20 ns
Satellite clock frequency bias error	< $3 \cdot 10^{-11}$

each antenna element’s signal is first filtered and amplified by its own RF chain (including a band-pass filter and Low-Noise Amplifier, LNA) and then down-converted via mixers to an intermediate frequency or base-band for sampling. High-speed Analogue-to-Digital Converters (ADCs) digitise each channel’s In-phase, Quadrature (I/Q) signal, and these digitised streams are combined in the digital domain using beamforming algorithms. By applying appropriate phase and amplitude weights to each channel, the receiver can electronically form directed beams — analogous to classical monopulse sum-and-difference patterns — to focus on signals from specific directions [12]. This DBF approach is crucial for improving sensitivity and spatial filtering; it maximises gain towards the targeted aircraft and suppresses interference, thereby enhancing SNR and enabling angle of arrival estimation. A common timing reference is shared across all channels, and the local oscillator and clock are derived from a single stable source, so that each channel’s sampling and phase are aligned. This strict timing alignment ensures that the multichannel system remains coherent, which is essential for the DBF process and for tagging each message with an accurate arrival time. Together, the DBF architecture and its carefully timed receiver chain allow the satellite ADS-B sensor to form multiple beams in different directions and reliably determine the AOA of incoming signals while simultaneously decoding ADS-B messages.

In [13–16] a detailed description of possible SATERA receiver chains and DBF antennas, can be found. In particular:

- the receiver chain was defined and the receiver sensitivity was fixed to -97 dBm (taking into account internal noise, receiver band, receiver configuration and losses);
- different antenna configurations were studied for the SATERA ADS-B receiver: truncated cone and truncated pyramid with 4 to 6 independent sectors, each sector with at least a panel of 4 by 4 radiation elements for vertical and horizontal beamforming, obtaining different performances in terms of beamwidth gain and antenna dimension (e.g. antenna gain between 12 and 17 dBi and radiation panel dimension of about 60×60 cm)
- TOA, AOA, and FOA measurement performance for different receiver and antenna configurations (instantaneous band, ADC number of bits, SNR) was evaluated;

The useful findings for this work are summarised in Table 2.

Beyond the core receiver chain, three additional supporting units are needed: the navigation unit, the timing unit, and the communication unit. The navigation unit is responsible for determining the satellite’s position, attitude and velocity in real-time. This unit typically integrates GNSS receivers (for example, GPS, Galileo), Inertial Navigation System (INS), and a dedicated Orbit Determination Sub-system (ODS). These elements provided the satellite position, velocity and attitude estimates required for referencing TOA, FOA, and AOA measurements to a precise spatial frame. Furthermore, this unit feeds critical state information into the signal processing chain, allowing

Doppler shifts and arrival angles to be interpreted in the context of satellite motion.

The performance of the satellite navigation unit for satellite position, velocity, and clock synchronisation errors is derived in [17], assuming a GNSS receiver, INS on board the satellite and an autonomous precise orbit determination exploiting sequential filtering. As per the attitude error, this was not considered in the mentioned document, but it is safe to assume that its value is negligible for the scope of this work, being much lower than the AOA receiver error. Indeed, the SATERA system includes a data network that uses laser ISLs. In order for these to function, star tracker-based attitude control is needed, which is characterised by very low errors, of the order of tens of μrad [18]. I.e., the AA-STR star tracker [19], already deployed on Iridium NEXT, could be used.

Concerning the accurate timing and synchronisation across the satellites, the timing unit generates all frequency and time references used throughout the payload. It features a highly stable oscillator, a reference clock, and a time and frequency estimator. This unit can leverage GNSS signals and/or inter-satellite synchronisation messages to discipline its internal time, achieving the strict coherence required for reliable TOA estimation, as described in [20], where it was shown that the clock bias error can span between 1 and 10 ns (nominal and faulty condition respectively) and the clock frequency bias ($\Delta f/f$) can span between $3 \cdot 10^{-12}$ and $3 \cdot 10^{-11}$.

Finally, the communication unit manages data exchange between satellites via ISLs and with the ground segment through DL. It is composed of dedicated transceivers, antennas, and modulation/demodulation systems designed to relay decoded ADS-B messages and extracted signal features to the CPS on Earth. This communication infrastructure ensures that multilateration and integrity monitoring can be performed on the ground using aggregated measurements from multiple satellites.

2.3. Communications network

The communication network facilitates the transfer of data from each receiving station to the CPS, where signal measurements are correlated and aircraft positions are computed. This network consists of two key subsystems: ISL and DL. ISL enables data relay between neighbouring satellites, ultimately routing the information to a satellite with ground station connectivity. Given that ATC operations are time-sensitive, the network must ensure low-latency delivery and synchronised reception of signals measured from the same emission. To prevent data age from exceeding the thresholds set by EUROCAE ED-142 A and ED-129C [21,22], the ISL subsystem will implement an adaptive routing algorithm to find the most efficient data path through the constellation. Finally, DL provides a direct radio connection between a satellite and a ground receiving station.

Defining the routing algorithm or the encoding, error correction, and data compression techniques of the network is out of the scope of this work, but a requirement on the network latency well below the requirement from the standard (ED-129C) was set (500 ms, instead of 1,5 s) also considering that the processing time in the CPS and the propagation time of the signal are well below this level.

2.4. CPS

The CPS receives data transmitted from the constellation and processes it to compute the position of the aircraft and to generate Target Reports (TRs) in ASTERIX Categories 20 and 21 [23,24], suitable for ATC use. Key CPS tasks include: correlating measurements from different satellites to the same aircraft emitter, solving a non-linear system of equations based on the most suitable set of measurements to independently estimate the aircraft position using advanced algorithms, tracking algorithms to refine position estimates, mitigate measurement noise, and derive additional parameters such as velocity and

acceleration, and finally computing the integrity test that compares GNSS-reported and MLAT-derived positions. The test provides a discrete scale that indicates the degree of discrepancy between the two. The last step is formatting of data according to the ASTERIX CAT020 (MLAT) and CAT021/053 (ADS-B) standards.

In the following, the CPS capability to compute the aircraft position will be studied to evaluate the possible performance of the proposed solution.

3. Satellite E-MLAT problem formulation

Assuming to have M satellites (also called anchors) that receive ADS-B signals from the aircraft, measure the signal parameters (e.g. TOA, FOA, AOA) and send this information to the CPS through ISL and DL, the localisation problem in the CPS consists of deriving the position of the aircraft, θ , using the previously mentioned measurements. Assuming that it is possible to have M different measurements from the M satellites in known positions, θ_i , the entire set of measurements, $\mathbf{m} = [m_1, m_2, \dots, m_M]^T$, also called observables, can be represented by the following general expression:

$$\mathbf{m} = \mathbf{f}(\theta) + \mathbf{n} = \begin{bmatrix} f_{11}(\theta) \\ f_{12}(\theta) \\ \vdots \\ f_{1N}(\theta) \\ f_{21}(\theta) \\ f_{22}(\theta) \\ \vdots \\ f_{2N}(\theta) \\ f_{M1}(\theta) \\ f_{M2}(\theta) \\ \vdots \\ f_{MN}(\theta) \end{bmatrix} + \begin{bmatrix} n_{11} \\ n_{12} \\ \vdots \\ n_{1N} \\ n_{21} \\ n_{22} \\ \vdots \\ n_{2N} \\ n_{M1} \\ n_{M2} \\ \vdots \\ n_{MN} \end{bmatrix} \quad (1)$$

where \mathbf{n} represents the measurement error and N is the number of unknowns in the vector θ .

The relationship between the position of the aircraft and the measurements is indicated by the function $\mathbf{f}(\theta)$, where $f_{ij}(\theta)$ is a function that depends on the spatial distribution of the satellites, that is, on the system geometry and on the type of measurements. The aim is to determine the position of the user, represented by the vector $\theta = [x, y, z]^T$ inverting the given system of equations.

More in detail, referring to Fig. 4, the positions of the satellites are denoted as $\theta_i = [x_i, y_i, z_i]^T$ for $i = 1, 2, \dots, M$ within a three-dimensional fixed coordinate reference frame, while the variable r_i represents the spatial distance between the aircraft and the i th satellite and R_i is the distance between the centre of the fixed reference frame and the satellite/aircraft.

It should be noted that the aircraft parameter vector θ may also include additional unknowns related to the aircraft parameters that need to be estimated, and the final localisation performance, commonly referred to as localisation accuracy, depends on the accuracy of the measurements (i.e., the n_i parameters) and the spatial distribution of the reference stations and the method used to solve the system for θ .

When measuring the time of arrival of the ADS-B signal at satellite i , the i th TOA measurement can be expressed as:

$$m_i^{TOA}(\theta) = TOA_i(\theta) + n_i^{TOA}(\theta) = \frac{1}{c} \sqrt{(x - x_i)^2 + (y - y_i)^2 + (z - z_i)^2} + dt_u + n_i^{TOA}(\theta) \quad (2)$$

where c is the speed of light; (x, y, z) are the aircraft coordinates; (x_i, y_i, z_i) are the coordinates of the i th satellite; dt_u is the user clock bias that takes into account the fact that the aircraft clock is not synchronised with the satellite clocks (assumed to be synchronised with each other); n_i^{TOA} is the TOA measurement error and it is given by the sum of all the error contribution in measuring the TOA, that are: satellite position errors, satellite synchronisation error, receiver measurement

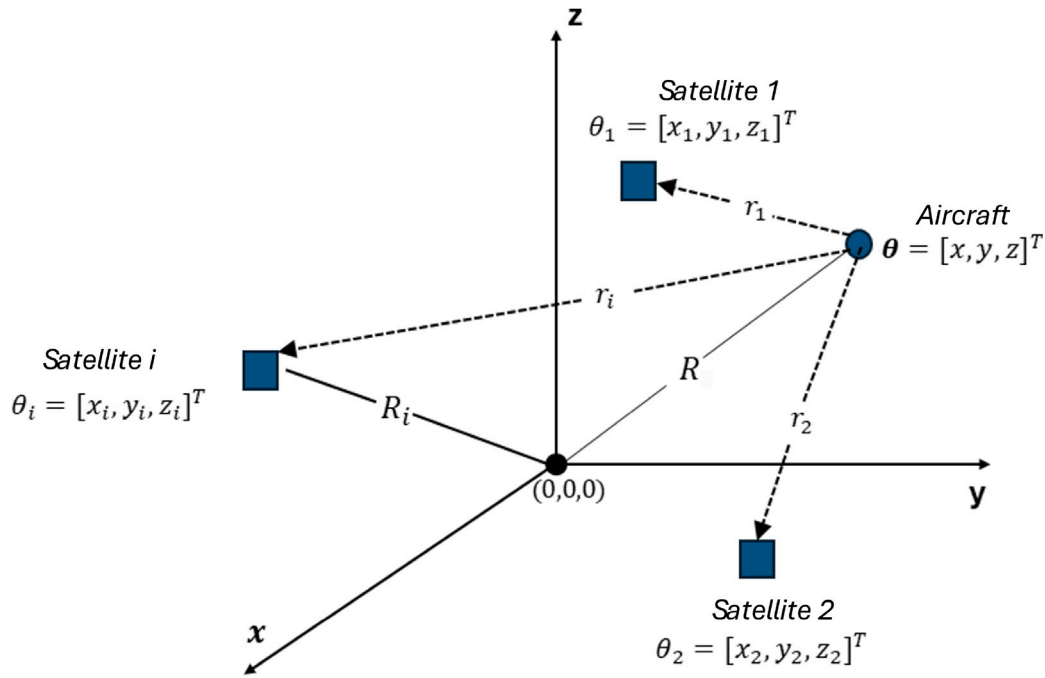


Fig. 4. Representation of the reference system and localisation setup.

errors and propagation error (mainly due to the ionosphere), the TOA error budget, discussed later, is reported in Table 4. It follows that the state vector to be estimated is composed of the aircraft coordinates and the aircraft clock bias:

$$\theta = [x, y, z, dt_u]^T \quad (3)$$

In case of FOA measurement, it is possible to recall that the measured received frequency is influenced by the Doppler effect [25]. The following approximation can be used to represent the received frequency:

$$f_{RX} = f_0 \left(1 + \frac{v_{rel}(\theta)}{c} \right) \quad (4)$$

where f_0 is the transmitted frequency and v_{rel} is expressed as:

$$v_{rel}(\theta) = \frac{(p_i - p) \cdot (v - v_i)}{r_i} \quad (5)$$

with p the aircraft position in (x, y, z) , v the aircraft velocity in (v_x, v_y, v_z) , p_i , v_i the i th satellite position and velocity and r_i the distance between the aircraft and the i th satellite.

Then, the i th FOA measurement can be expressed as:

$$m_i^{FOA}(\theta) = FOA_i(\theta) + n_i^{FOA}(\theta) = f_0 \left(\frac{v_{rel_i}(\theta)}{c} \right) + f_b + n_i^{FOA} \quad (6)$$

where f_b is the frequency bias due to the de-synchronisation between transmitter and receiver. As in the previous case, the satellites are synchronised with each other and the residual frequency bias error is taken into account in the error term n_i^{FOA} that is given by the sum of different error contributions: satellite velocity errors, measurement errors, synchronisation errors and propagation errors (see Table 4).

The corresponding aircraft state vector shall be composed of the aircraft position, velocity and frequency bias:

$$\theta = [x, y, z, v_x, v_y, v_z, f_b]^T \quad (7)$$

Finally, AOA measurements can be taken both horizontally and vertically.

The i th vertical AOA measurement can be expressed as:

$$m_i^{AOA,V}(\theta) = AOA_i^V(\theta) + n_i^{AOA,V}(\theta) =$$

$$\tan^{-1} \left(\frac{z - z_i}{\sqrt{(x - x_i)^2 + (y - y_i)^2}} \right) + n_i^{AOA,V}(\theta) \quad (8)$$

and the i th horizontal AOA measurement can be expressed as:

$$\begin{aligned} m_i^{AOA,H}(\theta) &= AOA_i^H(\theta) + n_i^{AOA,H}(\theta) = \\ &= \tan^{-1} \left(\frac{y - y_i}{x - x_i} \right) + n_i^{AOA,H}(\theta) \end{aligned} \quad (9)$$

and the corresponding state vector is composed of the aircraft coordinates $\theta = [x, y, z]^T$. Also in this case the n_i^{AOA} term collects all the error contributions in measuring the angle: the satellite attitude errors, the measurement error in the receiver and the propagation errors (see Table 4).

Note that, unlike time and frequency measurements, the observed AOA depends on the coordinates reference frame and the above formulations are given in the body frame of each satellite and not in the Earth-Centered Earth-Fixed (ECEF) reference frame used for a global surveillance system that has the origin in the centre of the Earth and the axis that rotate together with the rotation of the Earth.

More in details, the antenna bore-sight direction is defined in the satellite body frame, where it is assumed to be fixed and known. In principle, the relationship between the satellite body frame and any Earth-referenced frame is time-varying and depends on the satellite attitude as well as on Earth rotation effects.

Nevertheless, for the sake of simplicity, in this work we have used the NED frame to maintain the horizontal and vertical definition of the angles. This was done under the assumption that the transformation between the satellite body frame and the NED frame is available onboard. Such a transformation is assumed to implicitly account for all relevant effects, including satellite attitude dynamics and Earth rotation (e.g., through appropriate ECI-to-ECEF conversions). It can be easily obtained through a sequence of intermediate reference frame as:

$$v_{NED} = C_{ECEF}^{NED} C_{ECI}^{ECEF} C_B^{ECI} v_B \quad (10)$$

where v_B and v_{NED} are the vector representations in the body and NED frames, respectively, the rotation from the body frame to the Earth-Centered Inertial (ECI) frame is determined by the satellite attitude:

$$C_B^{ECI} = C(\text{attitude}) \quad (11)$$

and the transformation from ECI to Earth-Centered Earth-Fixed (ECEF) accounts for Earth rotation:

$$C_{ECI}^{ECEF} = \begin{bmatrix} \cos \theta_G & \sin \theta_G & 0 \\ -\sin \theta_G & \cos \theta_G & 0 \\ 0 & 0 & 1 \end{bmatrix} \quad (12)$$

where θ_G denotes the Greenwich Sidereal Time. Finally, the transformation from ECEF to the local NED frame, defined at latitude ϕ and longitude λ , is given by:

$$C_{ECEF}^{NED} = \begin{bmatrix} -\sin \phi \cos \lambda & -\sin \phi \sin \lambda & \cos \phi \\ -\sin \lambda & \cos \lambda & 0 \\ -\cos \phi \cos \lambda & -\cos \phi \sin \lambda & -\sin \phi \end{bmatrix} \quad (13)$$

where ϕ , λ are the NED frame's origin latitude and longitude that, in case of the SATERA system, are the latitude and longitude of the SATERA satellite (each satellite will have a different transformation matrix).

Last, note that the equations above can lead to singularities in certain specific points. To mitigate this problem, the *atan2* function [26] is used instead of the traditional *atan*:

$$\text{atan2}(y, x) = \begin{cases} \tan^{-1}\left(\frac{y}{x}\right) & \text{if } x > 0, \\ \tan^{-1}\left(\frac{y}{x}\right) + \pi & \text{if } x < 0 \wedge y \geq 0, \\ \tan^{-1}\left(\frac{y}{x}\right) - \pi & \text{if } x < 0 \wedge y < 0, \\ +\frac{\pi}{2} & \text{if } x = 0 \wedge y > 0, \\ -\frac{\pi}{2} & \text{if } x = 0 \wedge y < 0, \\ \text{undefined} & \text{if } x = 0 \wedge y = 0. \end{cases} \quad (14)$$

4. CRLB for satellite E-MLAT

A general approach to evaluating the performance of a localisation system is to assess its accuracy. Without committing to a specific estimator, it is possible to establish a lower bound for any unbiased estimator using the Cramér–Rao formulation [27]. The CRLB provides the theoretical minimum on the variance matrix of any unbiased estimator of a deterministic parameter for a given problem. Specifically, the variance of such an estimator cannot be smaller than the inverse of the Fisher Information [28]. An unbiased estimator that achieves this bound is said to be fully efficient. Such a solution minimises the mean squared error among all unbiased methods, making it the minimum-variance unbiased estimator [28].

Given an unknown parameter θ and a likelihood function $f(x; \theta)$ function of the random sample x , the CRLB states that the variance of any unbiased estimator $\hat{\theta}$ is at least equal to the inverse of the Fisher Information.

An example of such an estimator is the Iterative Weighted Least Squares (IWLS) estimator based on the Gauss–Newton method. It is generally biased due to the linearisation of the non-linear measurement model. However, under small-error conditions and with a sufficiently accurate initialisation, it can be considered approximately unbiased if the measurements themselves are unbiased or if their bias can be reduced by the use of models and/or calibration. In the authors' opinion, these assumptions are reasonable for obtaining a first-order estimate of the system accuracy, as also commonly adopted in [29–31] for GNSS systems, which are affected by errors of comparable order of magnitude in satellite position and velocity, synchronisation, and propagation (due to the use of similar frequency bands). Concerning the angle measurements, they can be considered unbiased if the antenna-receiver is equipped with a real-time calibration system. In fact, a DBF system can be calibrated by injecting a known reference signal across all receive channels, enabling the estimation and compensation of relative amplitude and phase. Typically, this procedure is performed periodically to account for environmental variations affecting the system [32,33].

Moreover, it can be easily shown that a common bias to all the measurements affects mainly the estimation of the transmitter clock time (and frequency) bias (not useful in SATERA), and not the estimation of the aircraft position.

It follows that, in the case of a multivariate Gaussian distribution with zero mean, the covariance is compared to the Fisher Information Matrix [27]:

$$\text{Cov}(\theta) = I(\theta)^{-1} \quad (15)$$

where the Fisher Information Matrix m, k element is:

$$I_{m,k} = H_m^T N(\theta)^{-1} H_k + \frac{1}{2} \text{tr} \left(N(\theta)^{-1} \frac{\partial N(\theta)}{\partial \theta_m} N(\theta)^{-1} \frac{\partial N(\theta)}{\partial \theta_k} \right) \quad (16)$$

When the covariance matrix of the measurement errors does not strongly depend on the state vector θ , the Fisher Information Matrix can be expressed as:

$$I(\theta) = H^T N(\theta)^{-1} H \quad (17)$$

where $N(\theta)$ is the covariance matrix of the measurement errors and H is the Jacobian matrix of the function $f(\theta)$. Note that H is a $M \times N$ matrix and N is a $M \times M$ matrix, where M is the number of measurements and N is the length of the state vector (or the number of unknown parameters), that changes depending on the chosen measurement types.

To derive a formulation for computing the CRLB, the H and N matrices are needed for each measurement type; their descriptions follow.

The Jacobian matrix for TOA measurements contains a row for each measurement or for each visible satellite:

$$H_{TOA} = \frac{1}{c} \begin{bmatrix} \frac{x-x_1}{r_1} & \frac{y-y_1}{r_1} & \frac{z-z_1}{r_1} & c \\ \frac{x-x_2}{r_2} & \frac{y-y_2}{r_2} & \frac{z-z_2}{r_2} & c \\ \vdots & \vdots & \vdots & \vdots \\ \frac{x-x_M}{r_M} & \frac{y-y_M}{r_M} & \frac{z-z_M}{r_M} & c \end{bmatrix} \quad (18)$$

where r_i is the distance between the aircraft and the i th satellite.

The measurement error covariance matrix is assumed to be diagonal, implying statistical independence among the measurements:

$$N_{TOA} = \begin{bmatrix} \sigma_{TOA_1}^2 & 0 & \dots & 0 \\ 0 & \sigma_{TOA_2}^2 & \dots & 0 \\ \vdots & \vdots & \ddots & \vdots \\ 0 & 0 & \dots & \sigma_{TOA_M}^2 \end{bmatrix} \quad (19)$$

where each $\sigma_{TOA_i}^2$ is the total measurement error variance of the TOA measurements and it takes into account for all the error contributions previously mentioned (receiver measurement error, ionospheric and tropospheric delay, satellite position error and satellite clock error).

This assumption simplifies the analysis but does not fully reflect the actual scenario, where TOA, FOA, and AOA measurements may exhibit common or highly correlated error sources. For example, propagation delays induced by the ionosphere and troposphere are typically correlated. However, the common additional bias affecting TOA and FOA measurements, introduced by the propagation medium, is indistinguishable from clock bias and clock frequency bias. Therefore, these effects mainly impact the estimation of such parameters, which are not exploited in the SATERA system, and thus have a negligible impact on localisation performance. Concerning the residual errors, due to correlated measurement conditions, they should be modelled by including off-diagonal terms in the covariance matrix.

Nevertheless, due to the complexity of accurately modelling the combined spatial effects of ionospheric and tropospheric variations, as well as satellite position and velocity errors, a first-order performance assessment can be obtained by approximating the covariance matrix as diagonal. This approach is, for example, consistent with standard practices in GNSS performance evaluation, where DOP or weighted DOP metrics are commonly adopted [29].

Substituting the above matrices in Eq. (17), it is possible to obtain the Fisher information matrix and, inverting it, the CRLB for the position estimation problem.

The Jacobian matrix for FOA measurements contains a row for each measurement, i.e., for each visible satellite. The full Jacobian matrix is composed of the partial derivatives of Eq. (6). The partial derivative with respect to coordinate x is (the derivatives with respect to y, z can be easily derived in a similar way):

$$\frac{\partial FOA_i}{\partial x}(\theta) = f_0 \cdot \frac{1}{c} \left[\frac{(v_{xi} - v_x)}{r_i} - \frac{v_{rel,i}(x - x_i)}{r_i^2} \right] \quad (20)$$

The partial derivative with respect to the velocity component v_x is (the derivatives with respect to v_y, v_z can be easily derived in the same way):

$$\frac{\partial FOA_i}{\partial v_x}(\theta) = f_0 \cdot \frac{1}{c} \cdot \frac{(x_i - x)}{r_i} \quad (21)$$

The partial derivative with respect to the frequency bias f_b is:

$$\frac{\partial FOA_i}{\partial f_b}(\theta) = 1 \quad (22)$$

Finally, the full Jacobian matrix becomes:

$$\mathbf{H}_{FOA} = \begin{bmatrix} \frac{\partial FOA_1(\theta)}{\partial x} & \dots & \frac{\partial FOA_1(\theta)}{\partial f_b} \\ \frac{\partial FOA_2(\theta)}{\partial x} & \dots & \frac{\partial FOA_2(\theta)}{\partial f_b} \\ \vdots & \ddots & \vdots \\ \frac{\partial FOA_M(\theta)}{\partial x} & \dots & \frac{\partial FOA_M(\theta)}{\partial f_b} \end{bmatrix} \quad (23)$$

Concerning the Error covariance matrix, with the same assumptions done before for TOA measurement, it can still be assumed diagonal, as measurements are statistically independent:

$$\mathbf{N}_{FOA} = \begin{bmatrix} \sigma_{FOA_1}^2 & 0 & \dots & 0 \\ 0 & \sigma_{FOA_2}^2 & \dots & 0 \\ \vdots & \vdots & \ddots & \vdots \\ 0 & 0 & \dots & \sigma_{FOA_M}^2 \end{bmatrix} \quad (24)$$

where each $\sigma_{FOA_i}^2$ is the total measurement error variance as the sum of the frequency error contributions, i.e., errors due to satellite velocity, propagation, measurement errors and synchronisation errors.

Substituting the above matrices in Eq. (17), it is possible to obtain the Fisher information matrix and, inverting it, the CRLB.

The Jacobian matrix for AOA measurements contains a row for each measurement. When both the vertical and horizontal AOA is measured, there will be two rows for each visible satellite:

$$\mathbf{H}_{AOA}(\theta) = \begin{bmatrix} -\frac{(x-x_1)(z-z_1)}{r_{H_1}^3} & -\frac{(y-y_1)(z-z_1)}{r_{H_1}^3} & \frac{1}{r_{H_1}} \\ \vdots & \vdots & \vdots \\ -\frac{(x-x_M)(z-z_M)}{r_{H_M}^3} & -\frac{(y-y_M)(z-z_M)}{r_{H_M}^3} & \frac{1}{r_{H_M}} \\ -\frac{y-y_1}{r_{H_1}^2} & \frac{x-x_1}{r_{H_1}^2} & 0 \\ \vdots & \vdots & \vdots \\ -\frac{y-y_M}{r_{H_M}^2} & \frac{x-x_M}{r_{H_M}^2} & 0 \end{bmatrix} \quad (25)$$

where the first M rows are related to the vertical AOA and the last M rows are related to the horizontal AOA. r_{H_i} is the horizontal distance between aircraft and i th satellite defined as $r_{H_i} = \sqrt{(x - x_i)^2 + (y - y_i)^2}$.

Since each satellite measures the AOA according to its own NED reference frame, the transformation matrix shown in Eq. (13) has to be applied, different for each satellite:

$$\mathbf{H}_{AOA_{ECEF}} = \begin{bmatrix} \mathbf{H}_{AOA_{ned_1}} \cdot \mathbf{C}_{ECEF}^{NED_1} \\ \mathbf{H}_{AOA_{ned_2}} \cdot \mathbf{C}_{ECEF}^{NED_2} \\ \vdots \\ \mathbf{H}_{AOA_{ned_M}} \cdot \mathbf{C}_{ECEF}^{NED_M} \end{bmatrix} \quad (26)$$

Assuming again that the measurement errors covariance matrix is diagonal, as measurements are statistically independent, it can be obtained by combining both vertical and horizontal measurement errors variances:

$$\mathbf{N}_{AOA}(\theta) = \begin{bmatrix} \mathbf{N}_{AOA,V}(\theta) & 0 \\ 0 & \mathbf{N}_{AOA,H}(\theta) \end{bmatrix} = \begin{bmatrix} \sigma_{AOA_1^V}^2 & 0 & \dots & \dots & \dots & 0 \\ \vdots & \ddots & \vdots & \vdots & \vdots & \vdots \\ 0 & \dots & \sigma_{AOA_M^V}^2 & \dots & \dots & 0 \\ 0 & \dots & \dots & \sigma_{AOA_1^H}^2 & \dots & 0 \\ \vdots & \vdots & \vdots & \vdots & \ddots & \vdots \\ 0 & 0 & \dots & 0 & \dots & \sigma_{AOA_M^H}^2 \end{bmatrix} \quad (27)$$

Substituting the above matrices in Eq. (17), it is possible to obtain the Fisher information matrix and, inverting it, the CRLB. Also in this case each element of the matrix \mathbf{N}_{AOA} take into account the propagation errors, the satellite attitude errors, and the measurement errors.

Last, but not least, multiple measurement types can be combined in the same system to improve accuracy and availability. To combine several measurements together, it is possible to stack the different measurement vectors in a final larger vector:

$$m = \begin{bmatrix} TOA_1 \\ \vdots \\ TOA_M \\ FOA_1 \\ \vdots \\ FOA_M \\ AOA_1 \\ \vdots \\ AOA_{2M} \end{bmatrix} + \begin{bmatrix} n_1^{TOA} \\ \vdots \\ n_M^{TOA} \\ n_1^{FOA} \\ \vdots \\ n_M^{FOA} \\ n_1^{AOA} \\ \vdots \\ n_{2M}^{AOA} \end{bmatrix} \quad (28)$$

The Jacobian is now obtained by computing the partial derivatives with respect to every unknown parameter, i.e., TOA measurements involve the clock bias dt_u , which was not present in FOA or AOA. Obviously, the partial derivatives with respect to parameters not originally present in a measurement definition are equal to 0. When all measurement types are combined, the resulting state vector is:

$$\theta = [x, y, z, v_x, v_y, v_z, dt_u, f_b]^T = [p, v, dt_u, f_b]^T \quad (29)$$

where

$$p = [x, y, z]^T, \quad v = [v_x, v_y, v_z]^T. \quad (30)$$

The final Jacobian matrix is:

$$\mathbf{H}^{TOA,FOA,AOA} = \begin{bmatrix} \mathbf{H}^{TOA} \\ \mathbf{H}^{FOA} \\ \mathbf{H}^{AOA} \end{bmatrix} = \begin{bmatrix} \frac{\partial TOA_1(\theta)}{\partial p} & 0 & \frac{\partial TOA_1(\theta)}{\partial dt_u} & 0 \\ \vdots & \vdots & \vdots & \vdots \\ \frac{\partial TOA_M(\theta)}{\partial p} & 0 & \frac{\partial TOA_M(\theta)}{\partial dt_u} & 0 \\ \frac{\partial FOA_1(\theta)}{\partial p} & \frac{\partial FOA_1(\theta)}{\partial v} & 0 & \frac{\partial FOA_1(\theta)}{\partial f_b} \\ \vdots & \vdots & \vdots & \vdots \\ \frac{\partial FOA_M(\theta)}{\partial p} & \frac{\partial FOA_M(\theta)}{\partial v} & 0 & \frac{\partial FOA_M(\theta)}{\partial f_b} \\ \frac{\partial AOA_1(\theta)}{\partial p} & 0 & 0 & 0 \\ \vdots & \vdots & \vdots & \vdots \\ \frac{\partial AOA_{2M}(\theta)}{\partial p} & 0 & 0 & 0 \end{bmatrix} \quad (31)$$

Finally, the position error is typically given in a local reference frame centred on the aircraft. The horizontal and vertical Root Mean Square (RMS) error shall be calculated by convention, assuming a local ENU (East-North-Up) system. The previously formulated CRLB, related

to the covariance matrix in the ECEF coordinates, can be converted to ENU applying the following rotation matrix:

$$\mathbf{C}_{ENU}^{ECEF} = \begin{bmatrix} -\sin\lambda & \cos\lambda & 0 \\ -\sin\phi\cos\lambda & -\sin\phi\sin\lambda & \cos\phi \\ \cos\phi\cos\lambda & \cos\phi\sin\lambda & \sin\phi \end{bmatrix} \quad (32)$$

where ϕ , λ are the ENU frame's origin latitude and longitude that, in the case of the SATERA system, are the latitude and longitude of the aircraft. Finally, the following formulation is used:

$$\mathbf{Cov}(\theta_{enu}) = \mathbf{C}_{ENU}^{ECEF} \mathbf{Cov}(\theta_{ecef}) \mathbf{C}_{ENU}^{ECEF^T} \quad (33)$$

The horizontal (H), vertical (V) and 3D RMS can be finally computed [29]:

$$RMS^H = \sqrt{\mathbf{Cov}_{11}(\theta_{enu}) + \mathbf{Cov}_{22}(\theta_{enu})} \quad (34)$$

$$RMS^V = \sqrt{\mathbf{Cov}_{33}(\theta_{enu})} \quad (35)$$

$$RMS^{3D} = \sqrt{\mathbf{Cov}_{11}(\theta_{enu}) + \mathbf{Cov}_{22}(\theta_{enu}) + \mathbf{Cov}_{33}(\theta_{enu})} \quad (36)$$

Note that the 3D RMS does not depend on the reference frame and that the result is the same if calculated using ECEF coordinates.

Last, a brief discussion of the contribution of different types of measurement on the final accuracy can be done observing the previous mentioned Fisher information matrices. In fact, using the chain rule, the Fisher Information Matrix (FIM) of the mixed mode can be decomposed as

$$\mathbf{I} = \mathbf{I}_{TOA} + \mathbf{I}_{AOA} + \mathbf{I}_{FOA} \quad (37)$$

and relevance of each measurement modality can be assessed by comparing the minimum eigenvalues of the corresponding FIM contributions. For TOA measurements, the FIM scales as

$$\mathbf{I}_{TOA} \sim \sum_i \frac{1}{\sigma_{TOA}^2 c^2} \mathbf{u}_i \mathbf{u}_i^T, \quad (38)$$

where \mathbf{u}_i , \mathbf{u}_i are the eigenvectors, which yields:

$$\lambda_{\min}(\mathbf{I}_{TOA}) \sim \frac{1}{\sigma_{TOA}^2 c^2} \quad (39)$$

with λ_{\min} the minimum eigenvalue. For AOA measurements, the FIM scales as

$$\mathbf{I}_{AOA} \sim \sum_i \frac{1}{\sigma_{AOA}^2 r^2} (\mathbf{I} - \mathbf{u}_i \mathbf{u}_i^T), \quad (40)$$

which yields

$$\lambda_{\min}(\mathbf{I}_{AOA}) \sim \frac{1}{\sigma_{AOA}^2 r^2}. \quad (41)$$

Finally, for FOA measurements, assuming Doppler sensitivity along the radial direction, the FIM scales as

$$\mathbf{I}_{FOA} \sim \sum_i \frac{1}{\sigma_{FOA}^2} \left(\frac{v_{rel} f_0}{rc} \right)^2 \mathbf{u}_i \mathbf{u}_i^T, \quad (42)$$

which yields

$$\lambda_{\min}(\mathbf{I}_{FOA}) \sim \frac{1}{\sigma_{FOA}^2} \left(\frac{v_{rel} f_0}{rc} \right)^2. \quad (43)$$

Comparing each contribution with TOA, we can define the sensitivity ratios:

$$\alpha_{AOA} \sim \frac{\lambda_{\min}(\mathbf{I}_{AOA})}{\lambda_{\min}(\mathbf{I}_{TOA})} = \frac{\sigma_{TOA}^2 c^2}{\sigma_{AOA}^2 r^2} \quad (44)$$

$$\alpha_{FOA} \sim \frac{\lambda_{\min}(\mathbf{I}_{FOA})}{\lambda_{\min}(\mathbf{I}_{TOA})} = \frac{\sigma_{TOA}^2 c^2}{\sigma_{FOA}^2} \left(\frac{v_{rel} f_0}{rc} \right)^2 \quad (45)$$

and imposing $\alpha_{AOA} \gtrsim 1$ and $\alpha_{FOA} \gtrsim 1$ yields the conditions:

$$\sigma_{AOA} \lesssim \frac{c}{r} \sigma_{TOA}, \quad \sigma_{FOA} \lesssim \frac{v_{rel} f_0}{r} \sigma_{TOA}. \quad (46)$$

These expressions show that AOA and FOA measurements are beneficial only when their induced transverse and Doppler-based localisation accuracies are comparable to or better than the radial accuracy provided by TOA. Note that this analysis is based on order-of-magnitude scaling arguments and assumes a well-conditioned geometry and statistically independent measurement modalities, it follows that comparison of minimum eigenvalues is intended as a heuristic metric to assess relative information content rather than an exact equality.

In the following section, different combinations and scenarios will be evaluated to assess the performance of the SATERA e-MLAT localisation.

5. Simulation and performance evaluation

In order to evaluate the performance of the proposed system, two different simulations were performed emulating different combinations of system parameters. The parameters of the simulated constellation are those listed in Section 2.1.

In the first evaluation, two trajectories covering the areas of interest of SATERA, the North Atlantic (NAT) corridor and the Europe to South America (EURSAM) corridor were evaluated. For the first, the trajectory connects New York, USA, to Madrid, Spain. For the second, the trajectory connects São Paulo, Brazil, to Milan, Italy. The EURSAM corridor, in particular, is more relevant for the purpose of this work, as it crosses the equator and the low latitudes. In this area, the satellites are farther apart, and coverage is poorer than in higher latitudes, affecting the overall system performance. For this reason and for the sake of brevity, only the EURSAM results are reported in Fig. 5.

A second simulation was performed, not considering a single trajectory but an entire area, to highlight the patterns of availability due to the constellation's motion; see Fig. 6. Note how the results are symmetrical with respect to the equator, so the figure only shows the northern half, up to 70°N. Indeed, the area of interest in SATERA comprises the latitudes between 70°S and 70°N.

For the system to be considered available, the horizontal accuracy is taken into account: the horizontal position error shall be lower than 350 m, according to the ATC requirements for en-route applications [21].

To determine which satellites are within the aircraft's field of view and can be used for measurements, the simulator employs a link budget analysis.

The power received on the satellite is defined as

$$PR = PT + GT + GR - LADD - A0 \quad (47)$$

Accounting for path loss, the chosen model is the Free-Space Path Loss (FSPL), where it is assumed that there are no obstacles between the satellites and the aircraft, except for the atmosphere. The FSPL equation is given by:

$$A0_{dB} = 20 \log \left(\frac{4\pi Rf}{c} \right) \quad (48)$$

where: R is the distance between the aircraft and the satellite, f is the ADS-B frequency (1090 MHz) and c is the speed of light in vacuum.

In the considered link budget, the additional loss parameter $LADD$ accounts for all the additional unmodelled losses due to the propagation (the multipath fading component has been assumed negligible, as reflections from atmospheric layers or the aircraft structure are considered irrelevant for this scenario, consequently, it is primarily determined by the propagation effects, such as ionospheric and tropospheric attenuation, possible multipath on the aircraft and Faraday rotation).

The gain of the receiver antenna GR is reported as a range, as different options are currently under studies, as previously mentioned.

The gain of the transmitter antenna GT was fixed at 3 dBi, knowing that, typically, two ADS-B blade antennas (approximately equivalent a quarter-wave monopole on a ground plane) are installed on the

Table 3
ADS-B receivers parameters.

Contribution	Value
TX antenna power (PT)	57 dBm [36]
RX antenna gain (GR)	12–17 dBi [14–16]
TX antenna gain (GT)	3 dBi
Additional losses (LADD)	3 dB
RX Sensitivity (S)	−97 dBm [13]

aircraft, one on the top and one on the bottom [34–36], and assuming that at least one is experiencing good geometry.

Having two antennas on board also significantly reduces the effects of aircraft manoeuvres (such as banking) on satellite visibility. For this reason, this problem is not taken into account at this stage.

Finally, if $PR \geq S$, and the satellite is over the horizon, it is considered in view.

Note that the receiver sensitivity S is derived taking into account the minimum signal to noise level useful for TOA, AOA and FOA estimation and to decode the ADS-B signal with a low BER and takes into account also for the internal losses of the receiver [13].

The parameters considered in the link budget are summarised in Table 3. They were derived from previous SATERA outputs, as discussed in Section 2.2.

The standard deviations of the measurement errors used to build the N matrix, as mentioned before, come from previous results of the project (receiver measurement errors [13], and satellite position and velocity errors [17] and synchronisation error [20]) or from the literature (atmospheric errors) [29–31,37] and their values reflect the contributions of different sources of error affecting each measurement, as shown in Table 4. Note that, for the scope of this work, the measurement error standard deviations are assumed to be constant. This greatly simplifies the CRLB computations at this stage and is a common assumption done for a first stage evaluation. Moreover, previous SATERA results [13] demonstrate that the TOA and FOA measurements are not significantly affected by variations in SNR if it is larger than 10 dB. More in detail, the position, the velocity and the attitude of the satellite are derived from typical values obtained using precise orbit determination exploiting inter satellite link, ground link, GNSS and on-board sensors such as the AA-STR star tracker [19]. Concerning the tropospheric and ionospheric errors standard deviations, they are obtained with the same assumption usually made for GNSS systems that operate on the same frequency band.

The presented scenarios were evaluated for three different operative configurations: using only TOAs; using TOAs plus additional FOAs and AOAs; and, finally, using only TOA while exploiting a higher antenna gain. The first two cases use a 12 dBi antenna, while the latter increases of only 2 dB, to a minimum of 14 dBi. Please note that we are simulating the change from 12 dBi to 14 dBi to evaluate the effect of the minimum gain that allows the capability to see always at least 4 satellites also taking into account the link budget. This means that introducing the best possible antenna configuration gives an additional 3 dB margin that can be useful to contrast not modelled losses (such as a lower GT due to the line of sight geometry).

The first test (classic MLAT system using only TOA measurements) was carried out using the parameters described above and, in particular, considering the receiver's antenna gain equal to 12 dBi and only TOA measurements were used. In this scenario, the number of visible satellites is often lower than 4, the minimum for TOA-based MLAT to work, causing the non-availability of the system.

The system was available (horizontal positional error lower than 350 m) 91.8% of the time over the NAT corridor and 57.4% of the time over the EURSAM corridor. See Table 5 for the availability comparison.

Fig. 5(a) shows the horizontal CRLB over the EURSAM trajectory. There are a high number of points in which the number of satellites is

lower than 4, not allowing a solution. When the satellites are 4 or more instead, the performance is well within the requirements.

The availability map (Fig. 6(a)) shows that the critical areas are those at lower latitudes as expected, explaining the lower performance over the EURSAM corridor.

The second test was carried out using again the same configuration, but this time also FOA and AOA measurements were used. The additional measurement types make it possible to compute a solution for the position estimate, even when the number of visible satellites is lower than 4.

In this case, the performance improved slightly, with the system available 92.8% of the time over the NAT corridor and 60.0% of the time over the EURSAM corridor. See Table 5 for the availability comparison.

Fig. 5(b) shows the horizontal CRLB over the EURSAM trajectory: where the satellites number is lower than 4, the use of FOA and AOA measurements allows to have a solution, but the error is almost always higher than the requirements. Moreover, when the satellites are 4 or more, the performance is the same as when using just TOA measurements. These results are also confirmed by Eq. (46), which for the specific case of SATERA yields the following maximum values for σ_{AOA} and σ_{FOA} to be useful for the position estimation (well below the actual value): $\sigma_{AOA} \approx 20 \mu\text{rad}$ and $\sigma_{FOA} \approx 91 \text{ Hz}$. These values were computed in the best case scenario, that is, the smallest possible distance for AOA (500 km), and the largest possible distance for FOA (3000 km), considering a satellite velocity of approximately 7600 m/s. Given that the system cannot achieve this precision, these measurements do not contribute significantly to localisation accuracy.

The availability map (Fig. 6(b)) shows that many of the critical areas are now covered (i.e., it is possible to compute the aircraft location), but the errors are high and the requirements are still not met.

The third test was carried out using again only TOA measurements, but considering the receiver's antenna gain improved from 12 dBi to 14 dBi. Thanks to the more favourable link budget configuration, more satellites are visible in all locations, almost always in a number of at least 4. The performance improvement is strong, with the system available 100.0% of the time over both the analysed trajectories. See Table 5 for the availability comparison.

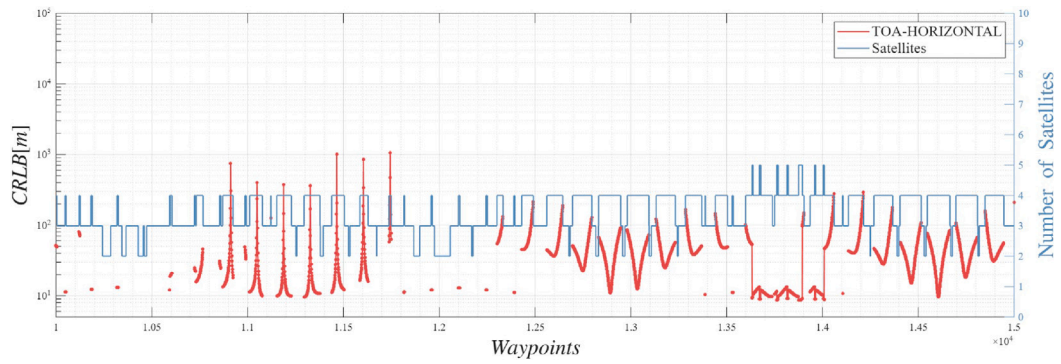
Finally, Fig. 5(c) shows the horizontal CRLB over the EURSAM trajectory. As the visible satellites are always 4 or more, the system seems to be always performing well. The estimated CRLB is almost always well below the requirements.

The availability map (Fig. 6(c)) shows that the requirements are met almost everywhere.

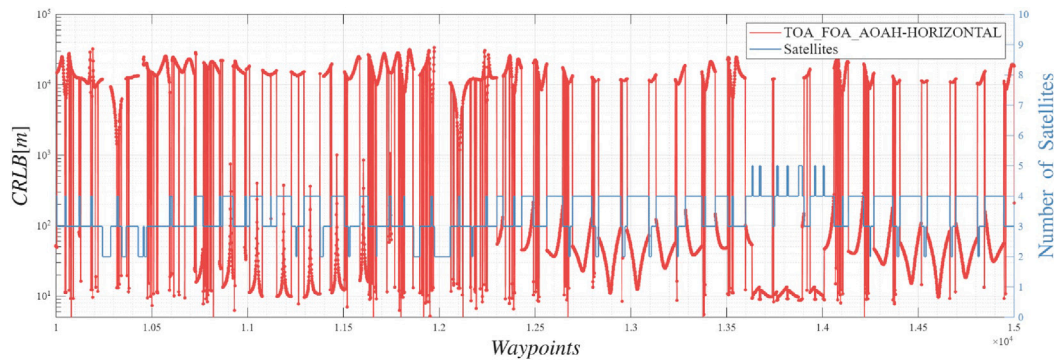
6. Discussion and conclusions

This paper presents a space-based MLAT system as part of the SATERA project, to be used as a GNSS-independent localisation system for aircraft. This can be used in remote areas, where ground-based MLAT is not available. The system is deployed on LEO satellites and was tested with TOA, FOA and AOA measurements. FOA and AOA measurements were added to improve the performance of the system, especially when the number of visible satellites is lower than 4, when TOA measurements alone cannot produce an estimate of the aircraft position. To test and compare the performances of the proposed solution with different configurations, the CRLB was used as an indicator of the achievable positioning accuracy. The evaluation showed that no relevant advantages were achieved in localisation accuracy with the addition of FOA and AOA measurements, as these are affected by much higher errors compared to the more precise TOA measurements. What has shown a much higher impact was the use of an enhanced receiver antenna to improve the available number of satellites for each position of the aircraft.

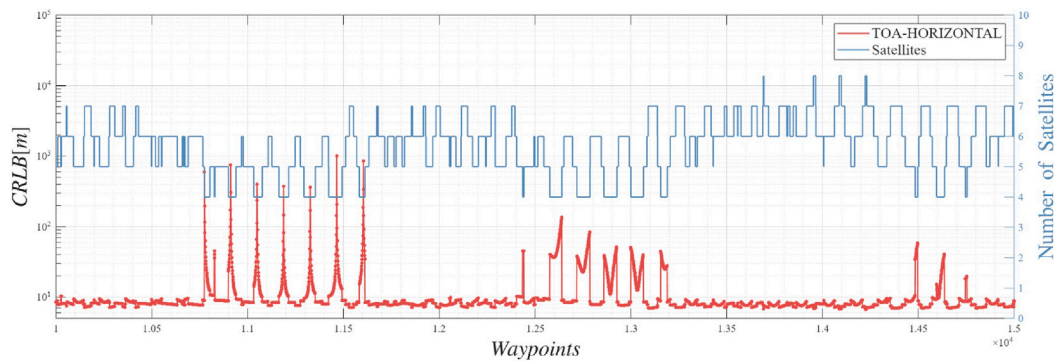
It is worth mentioning that while FOA and AOA measurements do not seem to improve the localisation performance, they offer other advantages, such as providing additional protection against spoofing



(a) TOA: 57.4% availability.



(b) TOA+FOA+AOA: 60.0% availability.



(c) TOA with improved receiver: 100.0% availability.

Fig. 5. CRLB over EURSAM corridor.

Table 4
Measurement errors standard deviations.

Measurement	TOA (ns)	FOA (Hz)	AOA (°)
Error sources (std.)	Ionosphere: 21 Troposphere: 3 Receiver: 15 Satellite position: 15 Satellite clock: 20	Ionosphere: 0.1 Troposphere: ≈0 Receiver: 500 Satellite velocity: 0.4 Satellite Clock Freq. Bias: ≈0	Ionosphere: <10'' Troposphere: ≈0 Receiver: 1 Satellite attitude: ≪1
Total (std.)	≈33	≈500	≈1

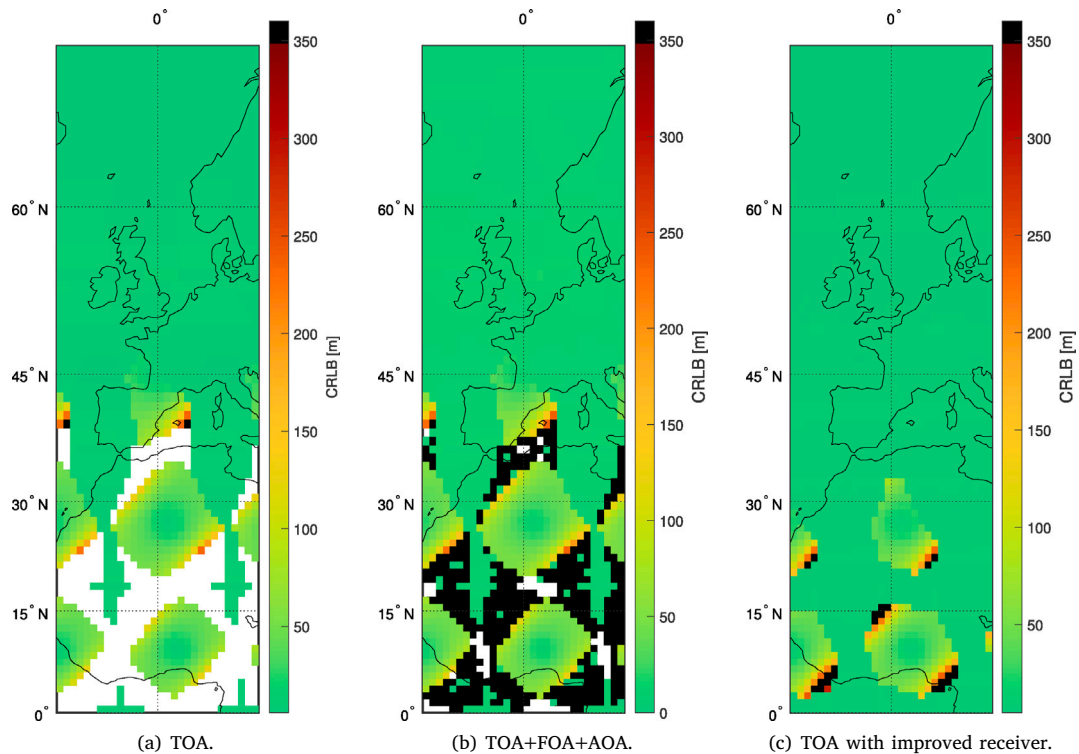


Fig. 6. CRLB over area.

Table 5

Availability of the system with different scenario configurations, over the NAT and EURSAM trajectories.

Availability	NAT	EURSAM
TOA	91.8%	57.4%
TOA+FOA+AOA	92.8%	60.0%
TOA+2 dB	100.0%	100.0%

or jamming attacks and improving resilience to both self and external interference.

To conclude, in this particular scenario, an improvement in the link budget configuration, such as exploiting a higher-gain antenna, has a much greater impact than the inclusion of multiple measurement types based on the frequency or angle of the received signal.

CRedit authorship contribution statement

Mauro Leonardi: Writing – review & editing, Writing – original draft, Validation, Supervision, Methodology, Investigation, Funding acquisition, Formal analysis, Conceptualization. **Giulio Sidoretti:** Writing – review & editing, Writing – original draft, Visualization, Validation, Software, Formal analysis. **Edoardo Navarra:** Writing – original draft, Validation, Software. **Mahsa Mohebbi:** Writing – review & editing, Writing – original draft.

Declaration of competing interest

The authors declare the following financial interests/personal relationships which may be considered as potential competing interests: Mauro Leonardi reports financial support was provided by SESAR. Giulio Sidoretti reports financial support was provided by SESAR. Mahsa Mohebbi reports financial support was provided by SESAR. If there are other authors, they declare that they have no known competing financial interests or personal relationships that could have appeared to influence the work reported in this paper.

Acknowledgements

This research was conducted within the framework of the SATERA project. SATERA has received funding from the SESAR 3 Joint Undertaking (JU) under grant agreement No 101164313. The JU receives support from the European Union’s Horizon Europe research and innovation programme and the SESAR 3 JU members other than the Union. The content of this paper reflects solely the views of its authors. The European Commission is not liable for any use that may be made of the information contained therein.

References

- [1] N.L. Fulton, Sensor-based situational awareness as a hazard paradigm for optimization of atc systems design, in: *Air Traffic Control Technologies*, Vol. 2464, SPIE, 1995, pp. 126–137.
- [2] J. Kuchar, A.C. Drumm, The traffic alert and collision avoidance system, *Linc. Lab. J.* 16 (2) (2007) 277.
- [3] B.S. Ali, *Aircraft Surveillance Systems: Radar Limitations and the Advent of the Automatic Dependent Surveillance Broadcast*, Routledge, 2017.
- [4] EUROCONTROL, Automatic dependent surveillance contract (ATS-B2), 2023, <https://www.eurocontrol.int/service/automatic-dependent-surveillance-contract-ats-b2>, (Accessed 31 March 2026).
- [5] EUROCONTROL, Automatic dependent surveillance- contract (ADS-C) factsheet, 2023.
- [6] Aireon, Aireon, 2023, <https://aireon.com/>, (Accessed 31 March 2026).
- [7] T.S. Consortium, Satera, 2025, www.satera-sesar.eu, (Accessed 23 August 2025).
- [8] E. Widdison, D.G. Long, A review of linear multilateration techniques and applications, *IEEE Access* 12 (2024) 26251–26266.
- [9] I.A. Mantilla-Gaviria, M. Leonardi, G. Galati, J.V. Balbastre-Tejedor, Time-difference-of-arrival regularised location estimator for multilateration systems, *IET Radar, Sonar & Navig.* 8 (5) (2014) 479–489.
- [10] M. Leonardi, A. Mathias, G. Galati, Two efficient localization algorithms for multilateration, *Int. J. Microw. Wirel. Technol.* 1 (3) (2009) 223–229.
- [11] X. Guo, Y. Zhou, J. Yang, Research on time synchronization method of ground-based navigation system, in: *China Satellite Navigation Conference (CSNC) 2015 Proceedings: Volume I*, Springer, 2015, pp. 529–536.
- [12] M. Skolnik, *Radar Handbook*, McGraw-Hill, 1990.
- [13] SATERA Consortium, Signal features extraction systems description, deliverable D3.1, 2025.

- [14] SATERA Consortium, Hybrid receiving station architecture, deliverable D3.2, 2025.
- [15] J. Vera-Sánchez, M. Ferrando-Rocher, G. Casasus-Goyeneche, M. Ferrando-Bataller, L-band unit-cell antenna design for satellite-based ads-b surveillance, in: 2025 IEEE International Symposium on Antennas and Propagation and North American Radio Science Meeting, AP-S/CNC-USNC-URSI, IEEE, 2025, pp. 1893–1895.
- [16] J. Vera-Sánchez, Á. Martín-Núñez, M. Ferrando-Rocher, M. Ferrando-Bataller, Circularly polarized conical array for ads-b applications in leo satellites, in: 2025 19th European Conference on Antennas and Propagation, EuCAP, IEEE, 2025, pp. 1–3.
- [17] SATERA Consortium, CRLB for MLAT, deliverable D5.2, 2025.
- [18] A. Lee, T. Hinderman, P. Serra, P. Forester, A. Gill, J. Conroy, C. Lisy, D. Coogan, L. Gallo, K. Cahoy, Optical alignment for cubesat crosslink laser communication terminals, in: Optical System Alignment, Tolerancing, and Verification XVI, Vol. 13602, SPIE, 2025, pp. 135–152.
- [19] Leonardo, AA-STR, 2022, <https://electronics.leonardo.com/en/products/aastr>, (Accessed 31 March 2026).
- [20] M. Leonardi, M. Mohebbi, G. Sidoretti, Robust and resilient gnss synchronization of leo satellites for space-based aircraft multilateration, in: 2025 IEEE 12th International Workshop on Metrology for AeroSpace, MetroAeroSpace, IEEE, 2025, pp. 654–659.
- [21] EUROCAE, Technical specification for wide area multilateration (WAM) systems, eD-142, 2023.
- [22] EUROCAE, Technical specification for a 1090 MHz extended squitter ADS-B surveillance system, eD-129C, 2023.
- [23] EUROCONTROL, Specification for surveillance data exchange ASTERIX part 14 category 20, cAT020, 2025.
- [24] EUROCONTROL, Specification for surveillance data exchange ASTERIX part 12 category 21, cAT021, 2025.
- [25] C.H. Papas, Theory of Electromagnetic Wave Propagation, Courier Corporation, 2014.
- [26] E.I. Organick, A FORTRAN Primer, in: Addison-Wesley series in computer science and information processing, Addison Wesley Longman Publishing, Co., Inc., 1966.
- [27] M.K. Steven, Fundamentals of Statistical Signal Processing, Vol. 10, PTR Prentice-Hall, Englewood Cliffs, NJ, 1993, p. 148, (151045).
- [28] G. Sirbu, Analysis and Evaluation of Positioning Systems for Lunar Navigation (Ph. D. thesis), University of Rome Tor Vergata, Rome, Italy, 2024.
- [29] E.D. Kaplan, C. Hegarty, Understanding GPS/GNSS: Principles and Applications, Artech house, 2017.
- [30] J.J. Spilker Jr., P. Axelrad, B.W. Parkinson, P. Enge, Global Positioning System: Theory and Applications, Vol. 1, American Institute of Aeronautics and Astronautics, 1996.
- [31] P.K. Enge, The global positioning system: Signals, measurements, and performance, Int. J. Wirel. Inf. Netw. 1 (2) (1994) 83–105.
- [32] M.R. Bell, Information Theory and Radar Waveform Design, IEEE Press/Wiley, Hoboken, NJ, USA, 2007.
- [33] K.F. Warnick, R. Maaskant, M.V. Ivashina, D.B. Davidson, Phased Arrays for Radio Astronomy, Remote Sensing, and Satellite Communications, Cambridge University Press, Cambridge, UK, 2018.
- [34] European Union Aviation Safety Agency, Airworthiness approval and operational criteria for ads-b out systems, in: Acceptable Means of Compliance AMC 20-24, European Union Aviation Safety Agency, Cologne, Germany, 2010, Guidance material for ADS-B Out certification and operational approval.
- [35] Federal Aviation Administration, Airworthiness approval of ads-b out systems, in: Advisory Circular AC 20-165B, U.S. Department of Transportation, Federal Aviation Administration, Washington, DC, USA, 2019, Advisory Circular providing guidance for certification of ADS-B Out systems.
- [36] International Civil Aviation Organization, Annex 10 to the convention on international civil aviation, in: Surveillance and Collision Avoidance Systems, Vol. IV, 2007.
- [37] B.A. Renfro, M. Stein, E.B. Reed, E.J. Villalba, An Analysis of Global Positioning System Standard Positioning Service Performance for 2020, Space and Geophysics Laboratory Applied Research Laboratories The University of Texas at Austin, 2021.